Distinct D-box Motifs in SPD-2 Mediate APC/C^{FZR-1}-Dependent Degradation and Centrosomal Localization in *Caenorhabditis elegans* Embryos

Running title: SPD-2 as a substrate of APC/C^{FZR-1}

Rachel N. Yim[1], Joseph R. DiPanni[1], Paollette A. Rivera[1], and Mi Hye Song[1,2]

[1]Department of Biological Sciences, Oakland University, Rochester, MI 48309, USA.
[2]Coresponding Author.

Contact Information: Mi Hye Song (msong2@oakland.edu)

Keywords: Anaphase Promoting Complex (APC/C); FZR-1; *C. elegans*; Centrosome; E3 Ubiquitin Ligase; SPD-2; ZYG-1; D-box; Degron; Proteasomal degradation

Abstract

Centrosome duplication must be tightly regulated to maintain genomic stability. In *Caenorhabditis elegans*, the APC/C and co-activator FZR-1 function as negative regulators of centrosome duplication by targeting specific substrates for proteolytic degradation. While *C. elegans* SAS-5 and ZYG-1 have been identified as substrates of APC/C^{FZR-1}, the mechanism by which APC/C^{FZR-1}-dependent degradation influences centrosome assembly remains unclear. Here, we identified SPD-2, the conserved homolog of human CEP192, as a substrate of APC/C^{FZR-1}. We show that loss of APC/C^{FZR-1} increases both cellular and centrosomal SPD-2 levels, and that SPD-2 physically associates with FZR-1 *in vivo*. Functional analyses of canonical D-box motifs reveal that D-box1, D-box2, and D-box3 each contribute to SPD-2 degradation, each with different functional consequences. Mutation of D-box3 alone partially rescued *zyg-1* mutant phenotypes by restoring centrosome duplication and embryonic viability through increased centrosomal SPD-2 and ZYG-1. In contrast, mutating D-box1 or D-box2 elevated cellular SPD-2 but did not rescue *zyg-1*, with the D-box1 mutation further reducing centrosomal SPD-2 and exacerbating duplication defects and lethality in *zyg-1* mutants. Our results reveal a conserved mechanism for APC/C^{FZR-1}-dependent degradation of SPD-2 and show that its degron motifs have dual functions in degradation and centrosomal localization, ensuring robust control of centrosome assembly during *C. elegans* embryogenesis.

Introduction

Centrosomes are the primary microtubule-organizing centers (MTOCs) in animal cells and play crucial roles in spindle assembly, chromosome segregation, and cell fate determination (Nigg and Holland 2018). Their functional capacity depends on the dynamic recruitment of pericentriolar material (PCM) around a centriole core, ensuring that centrosomes are competent for duplication and microtubule nucleation during each cell cycle. Errors in centrosome regulation can lead to defective mitotic spindles, genomic instability, and developmental disorders, including microcephaly and cancer (Fernandes-Mariano et al. 2025). Understanding how centrosome assembly and activity are coordinated in both time and space is therefore crucial in cell and developmental biology.

A key step in centrosome biogenesis and maturation in *Caenorhabditis elegans* is the recruitment of centrosome components to the site of new centriole formation, a process initiated by the conserved scaffold protein SPD-2 (Kemp et al. 2004; Pelletier et al. 2004) and its upstream factor SAS-7 (Sugioka et al. 2017). SPD-2 localizes to both centrioles and PCM, where it acts upstream of the kinase ZYG-1 (Pelletier et al. 2006; Shimanovskaya et al. 2014) and promotes the recruitment of SPD-5 and γ-tubulin to link PCM assembly with centriole duplication (Kemp et al. 2004; Pelletier et al. 2004). Loss of SPD-2 function significantly impairs centrosome biogenesis, maturation, and microtubule dynamics, underscoring its vital role in centrosome assembly and function (Kemp et al. 2004; Pelletier et al. 2004). Recent structural analyses have further uncovered the modular and intrinsically disordered structure of SPD-2, highlighting its capacity to mediate protein–protein interactions that link centrosome duplication with PCM expansion (Murph et al. 2022). Although SPD-2 is known to be crucial for centrosome regulation, its abundance and activity during centrosome assembly in *C. elegans* embryos remain unclear.

Proteolytic regulation by the anaphase-promoting complex/cyclosome (APC/C), an E3 ubiquitin ligase, has emerged as a key mechanism for controlling centrosome activity and maintaining centrosome copy number (Hames et al. 2001; Strnad et al. 2007; Arquint and Nigg 2014; Meghini et al. 2016; Medley et al. 2017; Medley et al. 2021; Tischer et al. 2022; Meghini et al. 2023). In *Drosophila*, the APC/C, in complex with its co-activator Fizzy-related (Fzr), targets Spd2 for degradation (Meghini et al. 2016). This degradation maintains centrosome asymmetry by limiting Spd2 accumulation at the daughter centrosome, ensuring proper PCM recruitment and maintaining spindle orientation. Without APC/C^{Fzr}-dependent proteolysis, excess Spd2 disrupts centrosome behavior, impairs microtubule nucleation, and randomizes the division axis (Meghini

et al. 2023). These findings demonstrate that proteasome-mediated turnover of conserved centrosome proteins is a crucial mechanism for maintaining centrosome function. Given the conserved role of SPD-2 in centrosome assembly, a similar APC/C-dependent regulation may occur in *C. elegans*. Indeed, SPD-2 functions upstream of ZYG-1 in the centrosome assembly pathway, indicating that precise regulation of SPD-2 levels is critical for promoting centrosome duplication and coordinating centrosome maturation (Kemp et al. 2004; Pelletier et al. 2004). Dysregulation of SPD-2 levels could therefore have serious consequences for centrosome assembly and function during the cell cycle.

In *C. elegans*, it has been shown that APC/C^{FZR-1} regulates centrosome duplication by promoting the degradation of the centrosome protein SAS-5 through its KEN-box motif (Medley et al. 2017) and by modulating centrosomal ZYG-1 levels via D-box motifs (Medley et al. 2021). Loss of FZR-1 or core APC/C subunits elevates SAS-5 and ZYG-1 levels at centrosomes, thereby restoring bipolar spindle formation in hypomorphic *zyg-1* mutants, revealing that APC/C^{FZR-1} functions at multiple points in the centrosome assembly pathway (Medley et al. 2017; Medley et al. 2021). Together, these genetic analyses indicate that APC/C^{FZR-1} targets multiple substrates, including ZYG-1 and SAS-5, as well as additional factors acting upstream of ZYG-1. Here, we investigate the hypothesis that APC/C^{FZR-1}-mediated degradation of SPD-2 provides a conserved mechanism to regulate centrosome assembly in *C. elegans* embryos.

Materials and Methods

C. elegans Culture and Genetic Analysis

The *C. elegans* strains used in this study are listed in Supplementary **Table 1**. All strains were derived from the wild-type Bristol N2 strain (Brenner 1974; Church et al. 1995) and maintained on MYOB plates seeded with Escherichia coli OP50 at 16°C or 20°C. Some strains were provided by the CGC, which is funded by NIH Office of Research Infrastructure Programs (P40 OD010440). For genetic analysis, individual L4 hermaphrodites were transferred to new plates and allowed to produce progeny for 0-24, 24-48, and 48-72 hours at the indicated temperatures. Progeny were allowed to develop for 18-24 hours before counting the number of larvae and dead eggs.

Immunofluorescence and Cytological analysis

Immunofluorescence and confocal microscopy were performed as described (Stubenvoll et al. 2016). The following primary and secondary antibodies were used at 1:3000 dilutions: DM1a (Millipore Sigma, #T9026), α-ZYG-1 (Stubenvoll et al. 2016), α-TBG-1 (Stubenvoll et al. 2016), α-

88 HA (Millipore Sigma, #11867423001, #11583816001; Thermo Fisher, #26183-A647), Alexa Fluor
89 488 and 568 secondary antibodies (Thermo Fisher, #A11001, A11004, A11006, A11034,
90 A11036). Confocal microscopy was performed using a Nikon Eclipse Ti-U microscope equipped
91 with a Plan Apo 60x1.4 NA lens, a Spinning Disk Confocal (CSU X1), and a Photometrics Evolve
92 512 camera. MetaMorph software (Molecular Devices, Sunnyvale, CA, USA) was employed for
93 image acquisition and fluorescence intensity quantification, and Adobe Photoshop/Illustrator 2025
94 were used for image processing. To quantify fluorescent signals at centrosomes, the average
95 intensity within an 8- or 9-pixel (1 pixel = 0.151 μm) diameter region was recorded from the
96 highest-intensity focal plane within an area centered on each centrosome. The average intensity
97 within a 25-pixel diameter region outside the embryo was used for background subtraction.
98
99 **CRISPR/Cas9 Genome Editing**
100 For genome editing, we used the co-CRISPR method described previously (Arribere et al. 2014;
101 Paix et al. 2015). crRNA was designed using the CRISPOR web server (crispor.tefor.net;
102 Concordet and Haeussler, 2018). Animals were microinjected with a mixture of commercially
103 available SpCas9 (IDT, Coralville, IA) and custom-designed oligonucleotides, including crRNAs
104 (Supplementary **Table 2**) at 0.4–0.8 mg/ml, tracrRNA at 12 mg/ml, and single-stranded DNA
105 oligonucleotides (Supplementary **Table 3**) at 25–100 ng/ml. The amount of crRNA was tripled for
106 low-efficiency crRNAs (SPD-2:D-box2). After injection, we screened for *dpy-10(cn64) II/+* rollers
107 in F1 progeny and genotyped F2. The genome editing was confirmed by Sanger sequencing
108 (GeneWiz, South Plainfield, NJ).
109
110 **Immunoprecipitation (IP) and Immunoblot**
111 IP experiments were performed as described previously (Medley et al. 2021). Embryos were
112 collected from young gravid worms using hypochlorite treatment (1:2:1 ratio of M9 buffer, 5.25%
113 sodium hypochlorite, and 5 M NaOH), frozen in liquid nitrogen, and stored at -80°C until use.
114 Embryos were suspended in lysis buffer [50 mM HEPES, pH 7.4, 2 mM EDTA, pH 8.0, 1 mM
115 $MgCl_2$, 150 mM KCl, 0.5 mM DTT, 0.5% NP-40 (v/v) and 10% glycerol (v/v)] with complete
116 protease inhibitor cocktail (Millipore Sigma) and MG132 (Tocris, Avonmouth, Bristol, UK), milled
117 for 8 minutes (repeat x2) at 30 Hz using a Retsch MM 400 mixer-mill (Verder Scientific, Newtown,
118 PA), then sonicated for 5 minutes in an ultrasonic bath (Thermo Fisher). Lysates were spun at
119 45,000 rpm for 45 minutes using a Sorvall RC M120EX ultracentrifuge (Thermo Fisher), and the
120 supernatant was recovered into clean tubes. An equal amount of total protein lysates was used
121 for each IP. Lysates and α-HA tag magnetic beads (MBL, #M181-11; Millipore Sigma, #SAE0197)

were incubated with rotation for 1 hour at 4°C and washed (5x 5 minutes) with PBST (PBS + 0.1% Tween-20). IP with beads and input samples were resuspended in 2X Laemmli Sample Buffer (Sigma) and boiled for 5 minutes before fractionation on a 4–12% NuPAGE Bis-Tris gel (Thermo Fisher Scientific). Proteins on a gel were transferred to a nitrocellulose membrane and analyzed using the antibodies at 1:3000- 10,000 dilutions: α-SPD-2 (Song et al., 2008), α-TBG-1 (Stubenvoll et al., 2016), DM1a (Sigma, #T9026), α-Ollas (Thermo Fisher, #MA5-16125), α-HA (Millipore Sigma, #11867423001, #11583816001), IRDye secondary antibodies (LI-COR Biosciences). Blots were imaged with the Odyssey M scanner (LI-COR Biosciences) and analyzed using Image Studio software (LI-COR Biosciences).

Statistical analysis

Statistics were produced using R statistical software and presented as average ± standard deviation (SD). Dot plots were generated using the R 'beeswarm' package. In the dotplots, the box ranges from the first through the third quartile of the data. The thick bar indicates the median. A solid grey line extends 1.5 times the interquartile range, or to the minimum and maximum data points. All P-values were calculated using two-tailed t-tests: ^{ns} $p>0.05$, * $p<0.05$, ** $p<0.01$, *** $p<0.001$.

Results and Discussion

Loss of FZR-1 stabilizes cellular SPD-2

In *C. elegans* embryos, APC/C^{FZR-1} negatively regulates centrosome duplication by promoting proteasomal degradation of SAS-5 (Medley et al. 2017) and by modulating centrosomal ZYG-1 levels (Medley et al. 2021). Previous genetic analyses indicate that APC/C^{FZR-1} targets multiple substrates, including ZYG-1 and SAS-5, as well as other factors acting upstream of ZYG-1 (Medley et al. 2021). Here, we investigate SPD-2, which functions upstream of ZYG-1 in the centrosome assembly pathway, as a potential substrate of APC/C^{FZR-1} in *C. elegans* embryos.

If APC/C^{FZR-1} directly targets SPD-2 for proteasomal degradation, then inhibiting APC/C^{FZR-1} should block SPD-2 degradation, thereby hyper-stabilizing SPD-2 and elevating its overall cellular levels. We first tested whether loss of APC/C^{FZR-1} affected SPD-2 abundance by quantitative Western blot analysis using anti-SPD-2 (Song et al. 2008) and protein lysates extracted from *fzr-1(bs31)* mutant (Medley et al. 2017) and wild-type (WT) embryos (**Fig. 1A**). Our quantification data showed that SPD-2 levels in *fzr-1(bs31)* mutant embryos are significantly higher (1.89±0.71-fold, $p<0.001$, n=27) compared to WT controls (1.00±0.0-fold, n=24), while *zyg-1* mutant embryos show no significant change (0.94±0.16-fold, n=10). In contrast, TBG-1 levels appear unaffected

156 in both mutants. We also observed a similar trend in *mat-3(or180)* for the core APC8/CDC23
157 subunit (Golden et al. 2000) and *emb-1(hc57)* mutants for the APC16 (Shakes et al. 2011) in the
158 *C. elegans* APC/C complex (Supplementary **Fig. 1A**). These findings indicate that loss of
159 APC/C^{FZR-1} results in elevated cellular SAS-5 levels, most likely due to increased protein stability
160 caused by impaired proteasomal degradation.
161
162 Then, increased levels of cellular SPD-2 in the embryo can influence the amount of SPD-2
163 recruited to centrosomes. To assess SPD-2 levels at centrosomes, we stained embryos with anti-
164 HA and measured the fluorescence intensity of the SPD-2::2xHA signal at centrosomes (Medley
165 et al. 2023). As SPD-2 localizes to both centrioles and PCM, we measured total centrosomal
166 (centriolar and PCM; **Fig. 1B**) and only centriolar SPD-2 signals (Supplementary **Fig. 1C**).
167 Quantitative immunofluorescence (IF) using SPD-2 tagged with 2xHA (SPD-2::2xHA) reveal that
168 during the first mitosis, *fzr-1(bs31)* mutant embryos exhibit increased levels of total centrosomal
169 SPD-2::2xHA (1.50±0.44-fold, n=92 at metaphase; 1.42±0.37-fold, n=39 at anaphase) compared
170 to WT controls (1.00±0.36-fold, n=47 at metaphase; 1.00±0.31-fold, n=33 at anaphase). A
171 comparable increase was seen in *mat-3(or180)* for the core APC8/CDC23 subunit (Golden et al.
172 2000) (Supplementary **Fig. 1B**). Additionally, a similar pattern was observed for the centriolar
173 SPD-2 levels (Supplementary **Fig. 1C**). The *fzr-1(bs31)* mutant embryo exhibits increased levels
174 of centriolar SPD-2::2xHA (1.50±0.37-fold, n=98 at metaphase; 1.36±0.44-fold, n=39 at
175 anaphase) compared to WT controls (1.00±0.19-fold, n=34 at metaphase; 1.00±0.30-fold, n=36
176 at anaphase). Since our prior study showed that *fzr-1(bs31)* mutant embryos display elevated
177 centrosomal ZYG-1 levels (Medley et al. 2021), we also measured ZYG-1 levels by co-staining
178 embryos with anti-HA and anti-ZYG-1 (Stubenvolle et al. 2016; **Fig. 1B**). Consistent with prior
179 observations, *fzr-1(bs31)* mutant embryos exhibit increased levels of centrosomal ZYG-1
180 (1.35±0.35-fold, n=80 at metaphase; 1.55±0.49-fold, n=31 at anaphase) compared to WT controls
181 (1.00±0.26-fold, n=31 at metaphase; 1.00±0.23-fold, n=32 at anaphase). Our data show that loss
182 of APC/C^{FZR-1} leads to a significant increase in both cellular and centrosomal levels of SPD-2,
183 supporting a model in which APC/C^{FZR-1}-dependent proteolysis regulates SPD-2 abundance
184 during *C. elegans* embryogenesis.
185
186 Furthermore, our immunoprecipitation (IP) assays demonstrate a physical interaction between
187 SPD-2 and FZR-1 *in vivo* (**Fig. 1C**). We detected SPD-2::2xHA and Ollas::FZR-1 in the pull-down
188 using embryonic lysates that express SPD-2::2xHA (Medley et al. 2023) and Ollas::FZR-1
189 (Medley et al. 2021). These results collectively support our hypothesis that APC/C^{FZR-1} directly

190 targets SPD-2 for proteasomal degradation. These findings support our model in which the APC/C
191 and its co-activator FZR-1 (APC/C^{FZR-1}) control SPD-2 levels in *C. elegans* embryos.
192
193 **SPD-2 contains five putative D-box motifs**
194 The E3 ubiquitin ligase APC/C^{FZR-1} targets specific substrates through the coactivator FZR-1,
195 which directly recognizes conserved motifs such as the destruction (D)-box and KEN-box within
196 the substrates (Glotzer et al. 1991; Pfleger and Kirschner 2000). Our *in silico* analysis identified
197 five potential D-box motifs (RxxL), but no KEN-box, within the *C. elegans* SPD-2 (**Fig. 2A**). In
198 SPD-2, D-box1 is located within the coiled-coil (CC3: aa291-322) domain, D-box2 within the
199 Aspm-SPD-2-Hydin (ASH) domain, D-box3 between the Ig-like and PDZ domains, and both D-
200 box4 and D-box5 within the PDZ domain (Murph et al. 2022). The sequence alignments indicate
201 that D-box4 is the only fully conserved motif across closely related nematodes, while the other
202 motifs retain partial but detectable sequence conservation (**Fig. 2B**).
203
204 We first examined whether APC/C^{FZR-1} targets SPD-2 by directly recognizing the canonical D-box
205 degron. To determine if any of the five putative D-box motifs function as degrons *in vivo* by
206 mediating FZR-1 and SPD-2 interaction, we used CRISPR/Cas9 genome editing to generate
207 degron mutants by substituting two key residues within each D-box motif (RxxL) with alanine
208 (AxxA) at their endogenous loci. Viable degron mutants were successfully produced for D-box1,
209 D-box2, and D-box3, each with two-alanine substitutions, referred to as the SPD-2:DB1(2A),
210 SPD-2:DB2(2A), and SPD-2:DB3(2A) mutations (**Table 1**). However, homozygous 2A mutations
211 in D-box4 and D-box5 were lethal, indicating that the normal function of these motifs is essential
212 for viability. Notably, a genome-wide genetic screen identified the *spd-2(oj29: R710Q)* mutation,
213 which alters the first Arg (R) residue of D-box4 (710-RTRL-713) and causes centrosome
214 duplication failure and embryonic lethality (**Fig. 2A**, Kemp et al. 2004). As a result, we were unable
215 to evaluate the functional roles of the D-box4 and D-box5 degron motifs *in vivo*. Due to this
216 limitation, we focused our analysis on D-boxes 1, 2, and 3 (DB1, 2, and 3) using viable degron
217 mutants to assess their functional effects in this study.
218
219 **Mutating the D-box leads to increased overall cellular SPD-2 levels**
220 If APC/C^{FZR-1} recognizes SPD-2 through its D-box motif, then mutating the D-box degron should
221 inhibit APC/C^{FZR-1} binding to SPD-2, preventing its degradation and resulting in higher SPD-2
222 protein levels. To assess how the D-box motif affects overall SPD-2 levels, we conducted
223 quantitative Western blot analysis using protein lysates from each degron mutant embryo

224 expressing SPD-2::2xHA (Medley et al. 2023) (**Fig. 2C**). Our results show that SPD-2 levels in all
225 three D-box mutant embryos are significantly higher (DB1: 1.72±0.43-fold, n=24; DB2: 2.10±0.57-
226 fold, n=17; DB3: 2.09±0.43-fold, n=11, $p<0.001$) compared to wild-type embryos (1.00±0.0-fold,
227 n=17). In contrast, TBG-1 levels remain unaffected in degron mutants. These findings suggest
228 that mutating the D-box motifs renders SPD-2 resistant to degradation, supporting the idea that
229 the three D-box motifs (DB1, DB2, and DB3) in SPD-2 function as degrons directly recognized by
230 APC/C^{FZR-1}. Blocking this recognition prevents SPD-2 degradation, leading to its accumulation
231 and mimicking SPD-2 overexpression.
232
233 **Only the SPD-2:DB3(2A) mutation results in elevated centrosomal SPD-2 levels**
234 Quantitative Western blot shows that the SPD-2 degron mutations lead to increased total SPD-2
235 levels in the embryo, consistent with enhanced protein stabilization. To assess whether this
236 stabilization influences SPD-2 levels at centrosomes, we examined how each degron mutation
237 changes centrosomal SPD-2 levels. We performed quantitative immunofluorescence (IF) to
238 compare centrosome-associated SPD-2 signals during the first mitosis in embryos expressing
239 SPD-2::2xHA, stained with anti-HA tag and anti-tubulin (Medley et al. 2021; **Fig. 2D**).
240
241 The DB3(2A) mutation resulted in elevated centrosomal SPD-2 levels (1.35±0.43-fold, $p<0.01$,
242 n=45 at metaphase; 1.32±0.42-fold, $p<0.0001$, n=34 at anaphase) compared to WT controls
243 (1.00±0.33-fold, n=60 at metaphase; 1.00±0.27-fold, n=38 at anaphase), indicating that mutating
244 the D-box3 does not impair centrosomal localization. Instead, the increased centrosomal signal
245 likely reflects the elevated pool of cellular SPD-2 caused by protein stabilization. In contrast, the
246 DB1(2A) mutation caused a significant decrease in centrosomal SPD-2 (0.59±0.20-fold, $p<0.001$,
247 n=28 at metaphase; 0.66±0.26-fold, $p<0.001$, n=10 at anaphase) compared to controls. This
248 dramatic reduction of centrosomal SPD-2 in the DB1(2A) mutant indicates that the D-box1 motif
249 is critical for SPD-2 localization to centrosomes, implicating its dual role as both a degron and a
250 key site for subcellular localization. Meanwhile, the DB2(2A) mutation caused no significant
251 changes in centrosomal SPD-2 (1.06±0.40-fold, $p=0.55$, n=21 at metaphase; 1.12±0.68-fold,
252 $p=0.40$, n=6 at anaphase) although the DB2(2A) mutation increases overall SPD-2 levels,
253 indicating that the SPD-2:DB2(2A) mutation partially impairs SPD-2 localization to centrosomes.
254 These degron mutants also showed consistent trends in centriolar SPD-2 levels (Supplementary
255 **Fig. 2A**). The DB3(2A) mutant embryos exhibit higher levels (1.23±0.28-fold, n=31 at metaphase;
256 1.13±0.22-fold, n=35 at anaphase), while the DB1(2A) mutants have reduced levels (0.57±0.18-
257 fold, n=28 at metaphase; 0.63±0.17-fold, n=10 at anaphase) and the DB2(2A) mutants show no

258 significant change (1.07±0.46-fold, n=21 at metaphase; 0.98±0.2-fold, n=8 at anaphase),
259 compared to WT controls (1.00±0.33-fold, n=56 at metaphase; 1.00±0.23-fold, n=27 at
260 anaphase).

261 Furthermore, to assess the impact of SPD-2 degron mutations on ZYG-1 recruitment, we
262 quantified centrosomal ZYG-1 levels in the degron mutants stained with anti-ZYG-1 and anti-
263 tubulin (**Fig. 2E**). Consistent with their elevated SPD-2 levels, DB3(2A) mutants exhibited a
264 significant increase in centrosomal ZYG-1 (1.14±0.29-fold, $p<0.01$, n=57 at metaphase;
265 1.21±0.21-fold, $p<0.001$, n=31 at anaphase) compared to WT controls (1.00±0.28-fold, n=72 at
266 metaphase; 1.00±0.25-fold, n=45 at anaphase). In contrast, DB1(2A) mutants, which display
267 reduced SPD-2 at centrosomes, showed a marked decrease in centrosomal ZYG-1 (0.50±0.13-
268 fold, $p<0.001$, n=24 at metaphase; 0.45±0.13-fold, $p<0.001$, n=19 at anaphase). DB2(2A) mutants
269 exhibited a slight reduction with no significant difference (0.84±0.10-fold, $p=0.07$, n=10 at
270 metaphase; 0.88±0.09-fold, $p=0.09$, n=14 at anaphase). These results align with the observed
271 patterns of centrosomal SPD-2 levels across the degron mutants (**Fig. 2D**). These data reveal a
272 strong correlation between centrosomal SPD-2 levels and ZYG-1 recruitment: mutants with
273 elevated centrosomal SPD-2 recruit more ZYG-1 to centrosomes, while those with reduced
274 centrosomal SPD-2 show a proportional decrease in ZYG-1.

275 **The SPD-2:DB3(2A) mutation leads to *zyg-1* suppression**

276 Next, we investigated how specific degron mutations affected SPD-2 activity in regulating
277 centrosome assembly, using the hypomorphic *zyg-1(it25)* genetic background. The *zyg-1(it25)*
278 allele carries a temperature-sensitive (ts) mutation (P442L) in the cryptic polo-box (CPB) domain,
279 which is critical for centrosomal recruitment of ZYG-1 (Kemphues et al. 1988; Shimanovskaya et
280 al. 2014). At the restrictive temperature 24°C, *zyg-1(it25*) mutant embryos fail to duplicate
281 centrosomes during the first mitosis, leading to monopolar spindle formation in the second mitosis
282 and resulting in 100% embryonic lethality (O'Connell et al. 2001). In the molecular hierarchy, SPD-
283 2 acts upstream of ZYG-1 and is required for ZYG-1 loading to centrioles before procentriole
284 formation (Pelletier et al. 2006).
285
286 If APC/C^{FZR-1} targets SPD-2 for degradation through its D-box degron, then mutating the D-box
287 motif should block APC/C^{FZR-1} binding, thus stabilizing SPD-2. Consequently, hyper-stabilized
288 SPD-2, similar to overexpression, could compensate for the reduced ZYG-1 activity in *zyg-1(it25)*
289 mutants. To determine whether any SPD-2 D-box mutation could rescue *zyg-1(it25)* phenotypes,
290 we introduced each mutation into the *zyg-1(it25)* background by genetic crossing and examined

291 their effects on embryonic survival (**Fig. 3A**, **Table 1**) and centrosome duplication (**Fig. 3B**).
292 Consistent with our hypothesis, the DB3(2A) mutation restored embryonic viability (35±16% vs
293 18±14%, $p<0.001$) and bipolar spindle formation (61±15% vs 34±22%, $p<0.01$) in *zyg-1(it25)*
294 mutants, compared to *zyg-1(it25)* controls, at the semi-restrictive temperature of 22.5°C. This
295 rescue effect was more potent at 22.5°C (34.5±15.9%) than at a more restrictive temperature of
296 23°C (5.0±4.3%; **Table 1**), suggesting that the SPD-2:DB3(2A) mutation depends on residual
297 ZYG-1 activity for suppression. However, suppression of *zyg-1* by the SPD-2:DB3(2A) mutation
298 appeared significantly weaker than that observed with the *fzr-1* mutation (100% bipolar spindles
299 and embryonic viability; **Fig. 3B, Table 1**) (Medley et al. 2021).
300
301 In contrast, the DB1(2A) mutation markedly decreased embryonic viability (0.5±0.9% vs 18±14%,
302 $p<0.001$; **Fig. 3A, Table 1**) and bipolar spindles (1.2±2.2% vs 34±22%, $p<0.001$; **Fig. 3B**) in *zyg-*
303 *1(it25)* mutants, although the DB1(2A) mutant alone remained largely viable (99.2±1.1%; **Table**
304 **1**). These results indicate that *zyg-1(it25)* provides a sensitized genetic background where SPD-
305 2:DB1(2A) causes near-complete lethality, demonstrating a strong synthetic effect. Similarly,
306 although *spd-2* and *zyg-1* mutations are individually recessive, *spd-2/+; zyg-1/+* double
307 heterozygotes exhibit ~75% embryonic lethality (Song et al. 2011). DB1(2A) mutant embryos
308 show centrosomal SPD-2 levels at 59% of those in wild-type embryos, comparable to those in
309 *spd-2* heterozygotes (*spd-2*/+), despite exhibiting elevated cellular SPD-2 levels. Thus, D-box1
310 appears to regulate centrosomal loading of SPD-2 independently of its degron function. Although
311 59% of centrosomal SPD-2 is sufficient to support ZYG-1 loading and normal centrosome
312 duplication in a wild-type background, combining the SPD-2:DB1(2A) mutation with homozygous
313 *zyg-1(it25)* severely disrupts centrosome duplication and mitosis, leading to near-complete
314 embryonic lethality at the semi-restrictive temperature (22.5 °C), where *zyg-1(it25)* alone causes
315 ~80% lethality (**Table 1**). These findings suggest that the D-box1 motif promotes proper
316 localization of SPD-2 at centrosomes and may facilitate its interaction with ZYG-1. D-box1 resides
317 within the coiled-coil (CC3) domain (**Fig. 2A**), and the DB1(2A) mutation consists of two alanine
318 substitutions (R298A and L301A). Since coiled-coil domains are known to mediate protein–protein
319 interactions (Murph et al. 2022), these substitutions likely impair the ability of SPD-2 to interact
320 with binding partners necessary for centrosome function.
321
322 Meanwhile, the DB2(2A) mutation had a minimal negative impact on embryonic viability
323 (14.4±17.6% vs 18±14%, $p=0.36$; **Table 1, Fig. 3A**) and bipolar spindle formation (30.2±18.5%
324 vs 34±22%, $p=0.55$; **Fig. 3B**) in *zyg-1(it25)* mutants. Like DB1(2A), the DB2(2A) mutation

325 increased overall SPD-2 levels but did not enhance its centrosomal activity, suggesting a partial
326 defect in SPD-2 loading, though much milder than DB2(2A). Since it resides within the ASH
327 domain, which is known to target SPD-2 to centrosomes (Murph et al. 2022), this may partly
328 explain the modest yet negative impact of the DB2(2A) mutation on embryonic viability, unlike its
329 effect on SPD-2 stability.
330
331 **Increased centrosomal ZYG-1 levels in SPD-2:DB3(2A) mutants**
332 In *zyg-1(it25)* embryos, centrosomal ZYG-1 is reduced to ~40% of WT controls (Medley et al.
333 2017), impairing the recruitment of SAS-5 and SAS-6, which are required for subsequent SAS-4
334 loading to centrosomes (Pelletier et al. 2006). Since SPD-2 acts upstream of ZYG-1 and promotes
335 centrosomal recruitment of ZYG-1, the observed suppression of *zyg-1* mutant phenotypes likely
336 results from increased centrosomal ZYG-1 levels caused by SPD-2 stabilization. Consequently,
337 increased levels of centrosomal ZYG-1 may restore the recruitment of downstream factors,
338 rendering centrosomes competent to assemble new centrioles in *zyg-1(it25)* mutants.
339
340 To assess how the SPD-2 degron mutation influenced ZYG-1 recruitment in *zyg-1(it25)* mutants,
341 we measured centrosomal ZYG-1 levels in *zyg-1(it25)* embryos carrying each degron mutation
342 (**Fig. 3C**). As expected, the SPD-2:DB3(2A) mutation led to increased centrosomal ZYG-1 levels
343 (1.15±0.22-fold, $p<0.001$, n=52 at metaphase; 1.20±0.29-fold, $p<0.001$, n=43 at anaphase)
344 compared to *zyg-1(it25)* controls (1.00±0.14-fold, n=44 at metaphase; 1.00±0.15-fold, n=33 at
345 anaphase). In contrast, the DB1(2A) mutation significantly decreased centrosomal ZYG-1
346 (0.53±0.14-fold, $p<0.001$, n=24 at metaphase; 0.31±0.06-fold, $p<0.001$, n=6 at anaphase), while
347 DB2(2A) mutants exhibited a slight decrease (0.92±0.18-fold, $p=0.466$, n=12 at metaphase;
348 0.91±0.29-fold, $p=0.02$, n=10 at anaphase). These results align with the patterns of centrosomal
349 SPD-2 levels across each degron mutant combined with *zyg-1(it25)* (Supplementary **Fig. 3A**).
350 The SPD-2:DB3(2A) mutation caused higher centrosomal SPD-2 levels (1.22±0.35-fold, $p<0.001$,
351 n=66 at metaphase; 1.25±0.28-fold, $p<0.001$, n=69 at anaphase), while DB1(2A) resulted in a
352 dramatic decrease (0.74±0.25-fold, $p<0.001$, n=22 at metaphase; 0.74±0.30-fold, $p<0.001$, n=33
353 at anaphase), and DB2(2A) showed a slight reduction (0.86±0.22-fold, $p<0.01$, n=42 at
354 metaphase; 1.03±0.24-fold, $p=0.67$, n=13 at anaphase), relative to *zyg-1(it25)* controls
355 (1.00±0.29-fold, n=76 at metaphase; 1.00±0.19-fold, n=30 at anaphase). These findings indicate
356 that the SPD-2:DB3(2A) mutation leads to increased centrosomal ZYG-1, which enhances the
357 recruitment of downstream factors and restores centrosome duplication and embryonic viability

358 in *zyg-1* mutants. This suggests a possible mechanism by which SPD-2:DB3(2A) suppresses the
359 *zyg-1* phenotype.
360
361 Finally, we observed that the SPD-2:DB3(2A) mutation results in lower centrosomal SPD-2 levels
362 than the *fzr-1(bs31)* mutation in *zyg-1(it25)* mutant backgrounds (1.25±0.28-fold, n=69 vs
363 2.59±0.89-fold, n=14, $p<0.001$; Supplementary **Fig. 3B**), consistent with the weaker suppression
364 of the *zyg-1* phenotype by the SPD-2:DB3(2A) mutation relative to the *fzr-1* mutation. SPD-
365 2:DB3(2A) mutant embryos show increased cellular SPD-2 levels, resulting in higher centrosomal
366 levels of SPD-2 and ZYG-1. However, the SPD-2:DB3(2A) mutation alone produces a much
367 weaker rescue of embryonic viability (1.25±0.28% vs 100%, **Table 1**) and bipolar spindle
368 formation (60±15% vs 100±0%, **Fig. 2B**) in *zyg-1(it25)* mutants compared to the *fzr-1* mutation.
369 Similar results were observed in our earlier studies, where ZYG-1 or SAS-5 degron mutations led
370 to *zyg-1* suppression that was less effective than the *fzr-1* mutation (Medley et al. 2017; Medley
371 et al. 2021). Several factors may account for the relatively weak suppression of *zyg-1* by the
372 DB3(2A) single mutation. First, we were unable to test the *in vivo* functions of D-box4 and D-box5
373 because their 2A substitutions are homozygous lethal, suggesting that these degrons may play a
374 more dominant role in SPD-2 turnover than D-box3. Second, we could not assess the combined
375 effects of D-boxes 1 through 3 on *zyg-1* suppression because D-box1 and D-box2 appear to be
376 required for centrosomal localization of SPD-2 and fail to rescue *zyg-1* phenotypes, making triple
377 mutant analysis challenging. Thus, the DB3(2A) mutation alone is unlikely to entirely block
378 APC/C^{FZR-1}-dependent degradation of SPD-2, resulting in only a partial rescue of the *zyg-1(it25)*
379 phenotype, which is weaker than the *fzr-1* mutation. Another possibility is that APC/C^{FZR-1} targets
380 additional centrosome proteins upstream of SPD-2, such as SAS-7 (Sugioka et al. 2017). In this
381 scenario, loss of APC/C^{FZR-1} would enhance ZYG-1 recruitment both by stabilizing ZYG-1 directly
382 and by increasing the levels of SPD-2 and other upstream factors, such as SAS-7, required for
383 ZYG-1 loading. However, testing the contribution of SAS-7 is beyond the scope of the present
384 study and will require additional investigation.
385
386 **SPD-2:DB1(2A) mutant embryos exhibit abnormal cell division patterns**
387 During our genetic analysis at 25°C, we observed a low but significant rate of embryonic lethality
388 in the SPD-2:DB1(2A) mutants, and this lethality was further exacerbated in the SPD-2:DB1(2A)
389 mutant embryos tagged with 2xHA (1.2% vs 4.8% lethality, **Table 1**). To investigate the cause of
390 embryonic lethality, we examined SPD-2:DB1(2A):2xHA mutant embryos stained for
391 centrosomes, microtubules, and DNA (**Fig. 4**). At 25°C, DB1(2A) mutant embryos display

392 abnormal cell division phenotypes. Consistent with reduced levels of SPD-2 (**Fig. 2D**) and ZYG-
393 1 (**Fig. 2E**) at centrosomes, these embryos display tiny and often highly asymmetric centrosomes
394 during the first mitotic metaphase. Such small and asymmetric centrosomes have also been
395 observed in ZYG-1:4D mutant embryos, which exhibit unstable and reduced levels of centrosomal
396 ZYG-1, indicating a partial block in centrosome duplication (Medley et al. 2023). DB1(2A) mutants
397 also display abnormal patterns in DNA segregation, cell division timing, and mitotic division
398 patterns, compared to the WT control, although at a low frequency (<5%, n>100). These cell
399 division defects likely account for embryonic lethality and further confirm that the D-box1 motif
400 functions not only as a degron motif but also plays a critical role in SPD-2 localization and its
401 centrosomal activity. Therefore, our study identified new key sites essential for SPD-2 activity in
402 regulating centrosome assembly during early embryonic development.
403
404 In summary, this study reports that *C. elegans* SPD-2 is a direct substrate of APC/C^{FZR-1} and
405 illustrates a regulatory network that links protein degradation, centrosomal localization, and
406 interactions with other partners. We showed that SPD-2 physically interacts with FZR-1 *in vivo*,
407 and that loss of APC/C^{FZR-1} results in elevated levels of both cellular and centrosomal SPD-2.
408 These results expand the repertoire of APC/C^{FZR-1} substrates beyond SAS-5 and ZYG-1 (Medley
409 et al. 2017; Medley et al. 2021), highlighting the crucial role of APC/C^{FZR-1} in controlling
410 centrosome assembly during *C. elegans* embryogenesis. Importantly, our findings also suggest
411 that APC/C^{FZR-1} may target additional centrosome factors, with SAS-7 (Sugioka et al. 2017) as a
412 strong candidate for future investigation.

413 Our degron motif analysis reveals both canonical and noncanonical functions. While all three D-
414 box mutations (DB1, DB2, and DB3) stabilize SPD-2, only the DB3 mutation restores centrosome
415 duplication and embryonic viability in *zyg-1* mutants. Our results also reveal that D-box1 and D-
416 box2 have functions beyond their roles as degron motifs. The D-box1 is required for efficient
417 centrosomal localization of SPD-2 and may facilitate its interaction with ZYG-1. Consistently,
418 DB1(2A) mutants show reduced centrosomal SPD-2 and ZYG-1 levels, leading to monopolar
419 spindle formation and increased embryonic lethality in *zyg-1* mutants. This suggests that D-box1
420 is important for both stabilizing and centrosomal targeting of SPD-2. By contrast, DB2 mutation
421 increased total SPD-2 levels but did not alter centrosomal pools or rescue *zyg-1* phenotypes.
422 These findings demonstrate that degron motifs serve multiple roles, with D-box1 and D-box2
423 involved in both proteasomal degradation and centrosomal functions.

424 Finally, our findings have broader evolutionary implications. SPD-2/CEP192 is a highly conserved
425 key regulator of centrosome assembly in metazoans (Kemp et al. 2004; Pelletier et al. 2004; Zhu
426 et al. 2008). Because dysregulation of centrosome factors is closely associated with genomic
427 instability and tumorigenesis in humans (Nigg and Holland 2018), understanding the degron-
428 dependent regulation of SPD-2/DSpd-2 in *C. elegans* and *Drosophila* (Meghini et al. 2016;
429 Meghini et al. 2023) provides an evolutionary framework for investigating analogous mechanisms
430 in human cells. Future work should explore how APC/C^{FZR-1} influences centrosome assembly and
431 microtubule dynamics, with potential implications for human health and cancer biology.

432

433 **Table 1. Genetic Analysis**

Strain	°C	% Embryonic viability (ave±sd)	n (progeny)
wild-type (N2)	25	99.8±0.3	2214
SPD-2$^{DB1(2A)}$		98.8±1.0*	2298
SPD-2$^{DB2(2A)}$		100.0±0.0	1224
SPD-2$^{DB3(2A)}$		99.9±0.2	2313
SPD-2::2xHA	25	99.2±0.7	2322
SPD-2$^{DB1(2A)}$::2xHA		95.2±2.7**	2124
SPD-2$^{DB2(2A)}$::2xHA		99.4±0.5	2431
SPD-2$^{DB3(2A)}$::2xHA		100.0±0.0**	1648
zyg-1(it25)	22.5	18.2±14.4	6053
SPD-2$^{DB1(2A)}$; zyg-1(it25)		0.5±0.9***	6249
SPD-2$^{DB2(2A)}$; zyg-1(it25)		14.4±17.6	4913
SPD-2$^{DB3(2A)}$; zyg-1(it25)		34.5±15.9***	6285
zyg-1(it25) fzr-1(bs31)		100.0±0.0***	1848
zyg-1(it25)	23	0.0±1.0	1163
SPD-2$^{DB1(2A)}$; zyg-1(it25)		0.0±0.0	859
SPD-2$^{DB2(2A)}$; zyg-1(it25)		0.0±0.6	710
SPD-2$^{DB3(2A)}$; zyg-1(it25)		5.0±4.3***	1095

434 *** $p<0.001$, ** $p<0.01$, * $p<0.05$, compared to the corresponding controls.

435

Data and Reagent Availability

The authors confirm that all data necessary to support the conclusions of the article are presented within the article, figures, tables, and supplementary material. Strains used in this study are available upon request.

Acknowledgements

We thank former and current members of the Song lab for their technical support. We especially thank WormBase and the *Caenorhabditis* Genetics Center (CGC). WormBase is supported by grant U24HG002223 from the National Human Genome Research Institute at the US National Institutes of Health, the UK Medical Research Council, and the UK Biotechnology and Biological Sciences Research Council. The CGC (St. Paul, MN), is funded by the National Institutes of Health Office of Research Infrastructure Programs (P40 OD010440).

Competing Interests

No competing interests declared.

Author Contributions

M.H.S. designed the experiments, wrote the manuscript, and performed quantifications of confocal imaging and protein levels from western blots. R.N.Y., J.D., P.R., and M.H.S. performed experiments and provided data.

Funding

This work was supported by a grant 1R15GM147857 to M.H.S. from the National Institute of General Medical Sciences. The funders had no role in study design, data collection and analysis, decision to publish, or manuscript preparation.

462 **References**

463 Arquint, C., and E. A. Nigg, 2014 STIL microcephaly mutations interfere with APC/C-mediated
464 degradation and cause centriole amplification. Curr Biol 24**:** 351-360.
465 Arribere, J. A., R. T. Bell, B. X. Fu, K. L. Artiles, P. S. Hartman *et al.*, 2014 Efficient marker-free
466 recovery of custom genetic modifications with CRISPR/Cas9 in Caenorhabditis elegans.
467 Genetics 198**:** 837-846.
468 Brenner, S., 1974 The genetics of Caenorhabditis elegans. Genetics 77**:** 71-94.
469 Church, D. L., K. L. Guan and E. J. Lambie, 1995 Three genes of the MAP kinase cascade,
470 mek-2, mpk-1/sur-1 and let-60 ras, are required for meiotic cell cycle progression in
471 Caenorhabditis elegans. Development 121**:** 2525-2535.
472 Fernandes-Mariano, C., J. N. Bugalhao, D. Santos and M. Bettencourt-Dias, 2025 Centrosome
473 biogenesis and maintenance in homeostasis and disease. Curr Opin Cell Biol 94**:**
474 102485.
475 Glotzer, M., A. W. Murray and M. W. Kirschner, 1991 Cyclin is degraded by the ubiquitin
476 pathway. Nature 349**:** 132-138.
477 Golden, A., P. L. Sadler, M. R. Wallenfang, J. M. Schumacher, D. R. Hamill *et al.*, 2000
478 Metaphase to anaphase (mat) transition-defective mutants in Caenorhabditis elegans. J
479 Cell Biol 151**:** 1469-1482.
480 Hames, R. S., S. L. Wattam, H. Yamano, R. Bacchieri and A. M. Fry, 2001 APC/C-mediated
481 destruction of the centrosomal kinase Nek2A occurs in early mitosis and depends upon
482 a cyclin A-type D-box. EMBO J 20**:** 7117-7127.
483 Kemp, C. A., K. R. Kopish, P. Zipperlen, J. Ahringer and K. F. O'Connell, 2004 Centrosome
484 Maturation and Duplication in C. elegans Require the Coiled-Coil Protein SPD-2. Dev
485 Cell 6**:** 511-523.
486 Kemphues, K. J., M. Kusch and N. Wolf, 1988 Maternal-effect lethal mutations on linkage group
487 II of Caenorhabditis elegans. Genetics 120**:** 977-986.
488 Medley, J. C., L. E. DeMeyer, M. M. Kabara and M. H. Song, 2017 APC/CFZR-1 Controls SAS-
489 5 Levels To Regulate Centrosome Duplication in Caenorhabditis elegans. G3
490 Genes|Genomes|Genetics 7**:** 3937-3946.
491 Medley, J. C., J. R. DiPanni, L. Schira, B. M. Shaffou, B. M. Sebou *et al.*, 2021 APC/CFZR-1
492 regulates centrosomal ZYG-1 to limit centrosome number. J Cell Sci 134.
493 Medley, J. C., R. N. Yim, J. DiPanni, B. Sebou, B. Shaffou *et al.*, 2023 Site-specific
494 phosphorylation of ZYG-1 regulates ZYG-1 stability and centrosome number. iScience
495 26**:** 108410.

496 Meghini, F., T. Martins, X. Tait, K. Fujimitsu, H. Yamano *et al.*, 2016 Targeting of Fzr/Cdh1 for
497 timely activation of the APC/C at the centrosome during mitotic exit. Nat Commun 7**:**
498 12607.
499 Meghini, F., T. Martins, Q. Zhang, N. Loyer, M. Trickey *et al.*, 2023 APC/C-dependent
500 degradation of Spd2 regulates centrosome asymmetry in Drosophila neural stem cells.
501 EMBO Rep 24**:** e55607.
502 Murph, M., S. Singh and M. Schvarzstein, 2022 A combined in silico and in vivo approach to the
503 structure-function annotation of SPD-2 provides mechanistic insight into its functional
504 diversity. Cell Cycle 21**:** 1958-1979.
505 Nigg, E. A., and A. J. Holland, 2018 Once and only once: mechanisms of centriole duplication
506 and their deregulation in disease. Nat Rev Mol Cell Biol 19**:** 297-312.
507 O'Connell, K. F., C. Caron, K. R. Kopish, D. D. Hurd, K. J. Kemphues *et al.*, 2001 The C.
508 elegans zyg-1 gene encodes a regulator of centrosome duplication with distinct maternal
509 and paternal roles in the embryo. Cell 105**:** 547-558.
510 Paix, A., A. Folkmann, D. Rasoloson and G. Seydoux, 2015 High Efficiency, Homology-Directed
511 Genome Editing in Caenorhabditis elegans Using CRISPR-Cas9 Ribonucleoprotein
512 Complexes. Genetics 201**:** 47-54.
513 Pelletier, L., E. O'Toole, A. Schwager, A. A. Hyman and T. Muller-Reichert, 2006 Centriole
514 assembly in Caenorhabditis elegans. Nature 444**:** 619-623.
515 Pelletier, L., N. Ozlu, E. Hannak, C. Cowan, B. Habermann *et al.*, 2004 The Caenorhabditis
516 elegans centrosomal protein SPD-2 is required for both pericentriolar material
517 recruitment and centriole duplication. Curr Biol 14**:** 863-873.
518 Pfleger, C. M., and M. W. Kirschner, 2000 The KEN box: an APC recognition signal distinct from
519 the D box targeted by Cdh1. Genes Dev 14**:** 655-665.
520 Shakes, D. C., A. K. Allen, K. M. Albert and A. Golden, 2011 emb-1 encodes the APC16 subunit
521 of the Caenorhabditis elegans anaphase-promoting complex. Genetics 189**:** 549-560.
522 Shimanovskaya, E., V. Viscardi, J. Lesigang, M. M. Lettman, R. Qiao *et al.*, 2014 Structure of
523 the C. elegans ZYG-1 cryptic polo box suggests a conserved mechanism for centriolar
524 docking of Plk4 kinases. Structure 22**:** 1090-1104.
525 Song, M. H., L. Aravind, T. Muller-Reichert and K. F. O'Connell, 2008 The conserved protein
526 SZY-20 opposes the Plk4-related kinase ZYG-1 to limit centrosome size. Dev Cell 15**:**
527 901-912.

528 Song, M. H., Y. Liu, D. E. Anderson, W. J. Jahng and K. F. O'Connell, 2011 Protein
529 phosphatase 2A-SUR-6/B55 regulates centriole duplication in C. elegans by controlling
530 the levels of centriole assembly factors. Dev Cell 20**:** 563-571.
531 Strnad, P., S. Leidel, T. Vinogradova, U. Euteneuer, A. Khodjakov *et al.*, 2007 Regulated
532 HsSAS-6 levels ensure formation of a single procentriole per centriole during the
533 centrosome duplication cycle. Dev Cell 13**:** 203-213.
534 Stubenvoll, M. D., J. C. Medley, M. Irwin and M. H. Song, 2016 ATX-2, the C. elegans Ortholog
535 of Human Ataxin-2, Regulates Centrosome Size and Microtubule Dynamics. PLoS
536 Genet 12**:** e1006370.
537 Sugioka, K., D. R. Hamill, J. B. Lowry, M. E. McNeely, M. Enrick *et al.*, 2017 Centriolar SAS-7
538 acts upstream of SPD-2 to regulate centriole assembly and pericentriolar material
539 formation. Elife 6.
540 Tischer, T., J. Yang and D. Barford, 2022 The APC/C targets the Cep152-Cep63 complex at the
541 centrosome to regulate mitotic spindle assembly. J Cell Sci 135.
542 Zhu, F., S. Lawo, A. Bird, D. Pinchev, A. Ralph *et al.*, 2008 The mammalian SPD-2 ortholog
543 Cep192 regulates centrosome biogenesis. Curr Biol 18**:** 136-141.
544

545

546 **Figure Legends**

547 **Figure 1. Loss of FZR-1 stabilizes SPD-2.** (**A**) Representative western blot with anti-SPD-2 and
548 anti-TBG-1 using embryonic lysates extracted from *fzr-1(bs31)* mutants, wild-type(*N2*), and *zyg-*
549 *1(it25)* mutants (Left). Tubulin was used as a loading control. Quantitative Western blot analyses
550 show significantly increased levels of SPD-2 (Middle) in *fzr-1(bs31)* mutants (1.89±0.71-fold,
551 $p<0.001$, n=27), but no change in *zyg-1(it25)* mutants (0.94±0.16-fold, $p=0.49$, n=10), compared
552 to wild-type (WT) controls (1.00±0.0-fold, n=24). In contrast, there were no significant differences
553 in TBG-1 levels (Right) among *fzr-1(bs31)* mutants (1.01±0.12-fold, $p=0.80$, n=14), *zyg-1(it25)*
554 mutants (1.01±0.07-fold, $p=0.53$, n=15), and wild-type controls (1.00±0.0-fold, n=15). (**B**) (Top)
555 Quantification of total centrosomal SPD-2::2xHA and ZYG-1 levels during the first mitotic cycle.
556 Each dot represents a centrosome. (Bottom) Embryos stained for SPD-2::2xHA and ZYG-1 at the
557 first mitotic metaphase and anaphase, with magnified images of posterior centrosomes. Bars, 10
558 μm. In the plots, the box ranges from the first through the third quartile of the data. The thick bar
559 indicates the median. (**A-B**) The solid grey line extends 1.5 times the interquartile range or to the
560 minimum and maximum data points. $^{ns}p>0.05$, $^{***}p<0.001$ (two-tailed t-tests). (**C**) IP using anti-
561 HA suggests that SPD-2 physically interacts with FZR-1. Protein lysates extracted from embryos
562 expressing only Ollas::FZR-1 were used as a negative control; ~1% of the total lysates were
563 loaded in the input lanes. Tubulin was used as a loading control in the input lanes.

564

565 **Figure 2. Mutating D-box motifs elevates overall cellular levels of SPD-2.** (**A**) The SPD-2
566 protein structure illustrates the locations of D-boxes (DB:1 through 5), functional domains, and
567 mutant alleles. (**B**) Sequence alignments of D-box motifs in the *Caenorhabditis* species. (**C**) (Left)
568 Representative western blot with anti-HA and anti-TBG-1 using embryonic lysates from individual
569 degron mutants and wild-type (WT) controls expressing SPD-2::2xHA. Tubulin was used as a
570 loading control. (Middle) Quantitative western blot analysis shows significantly increased levels
571 of SPD-2::2xHA in all three degron mutants. (Right) In contrast, there were no significant
572 differences in TBG-1 levels among the degron mutants and wild-type controls. (**D-E**) (Left)
573 Quantification of total centrosomal SPD-2::2xHA levels during the first mitotic cycle. Each dot
574 represents a centrosome. (Right) Embryos stained for (**D**) SPD-2::2xHA and (**E**) ZYG-1 at the first
575 mitotic metaphase and anaphase, with magnified images of posterior centrosomes. Bars, 10 μm.
576 (**C-E**) In the plots, the box ranges from the first through the third quartile of the data. The thick bar
577 indicates the median. The solid grey line extends 1.5 times the interquartile range or to the
578 minimum and maximum data points. $^{ns}p>0.05$, $^{**}p<0.01$, $^{***}p<0.001$ (two-tailed t-tests).

579

580 **Figure 3. Mutating SPD-2 D-box3 leads to the suppression of *zyg-1* phenotypes and**
581 **increased centrosomal ZYG-1 levels.** (**A**) Embryonic viability at 22.5°C (See **Table 1**). Each dot
582 represents a hermaphrodite. (**B**) Quantification of monopolar (dark grey) and bipolar (light grey)
583 spindles in two-cell stage embryos at 23°C. Average and standard deviation (SD) are presented.
584 n is the number of blastomeres. Embryos stained for centrosomes (TBG-1), microtubules, and
585 DNA, illustrate mitotic spindles at the second mitosis. (**C**) (Left) Quantification of centrosome-
586 associated ZYG-1 levels at the first mitotic metaphase and anaphase in *zyg-1(it25)* mutant
587 backgrounds with individual degron mutations. Each dot represents a centrosome. (Right)
588 Embryos stained for ZYG-1 and microtubules during the first mitotic cycle, with magnified images
589 of posterior centrosomes. (**B-C**) Bars, 10 μm. (**A,C**) In the plots, the box ranges from the first
590 through the third quartile of the data. The thick bar indicates the median. A solid grey line extends
591 1.5 times the interquartile range, or to the minimum and maximum data points. (**A-C**) $^{ns}p>0.05$,
592 $^{*}p<0.05$, $^{**}p<0.01$, $^{***}p<0.001$ (two-tailed t-tests).
593
594 **Figure 4. SPD-2:DB1(2A) mutants exhibit cell division defects during early embryogenesis.**
595 Embryos expressing SPD-2::2xHA stained for centrosomes (SAS-4), microtubules, and DNA. At
596 25°C, SPD-2:DB1(2A) mutant embryos exhibit abnormal cell division phenotypes, including small
597 centrosomes and highly asymmetric centrosome sizes during the first mitotic metaphase, DNA
598 missegregation (arrowhead), synchronous mitotic timing, and aberrant patterns of mitotic
599 divisions, compared to the WT embryos (Top). Bar, 10 μm.
600
601
602

Figures 1-4 Yim et al. 2025

Figure 1.

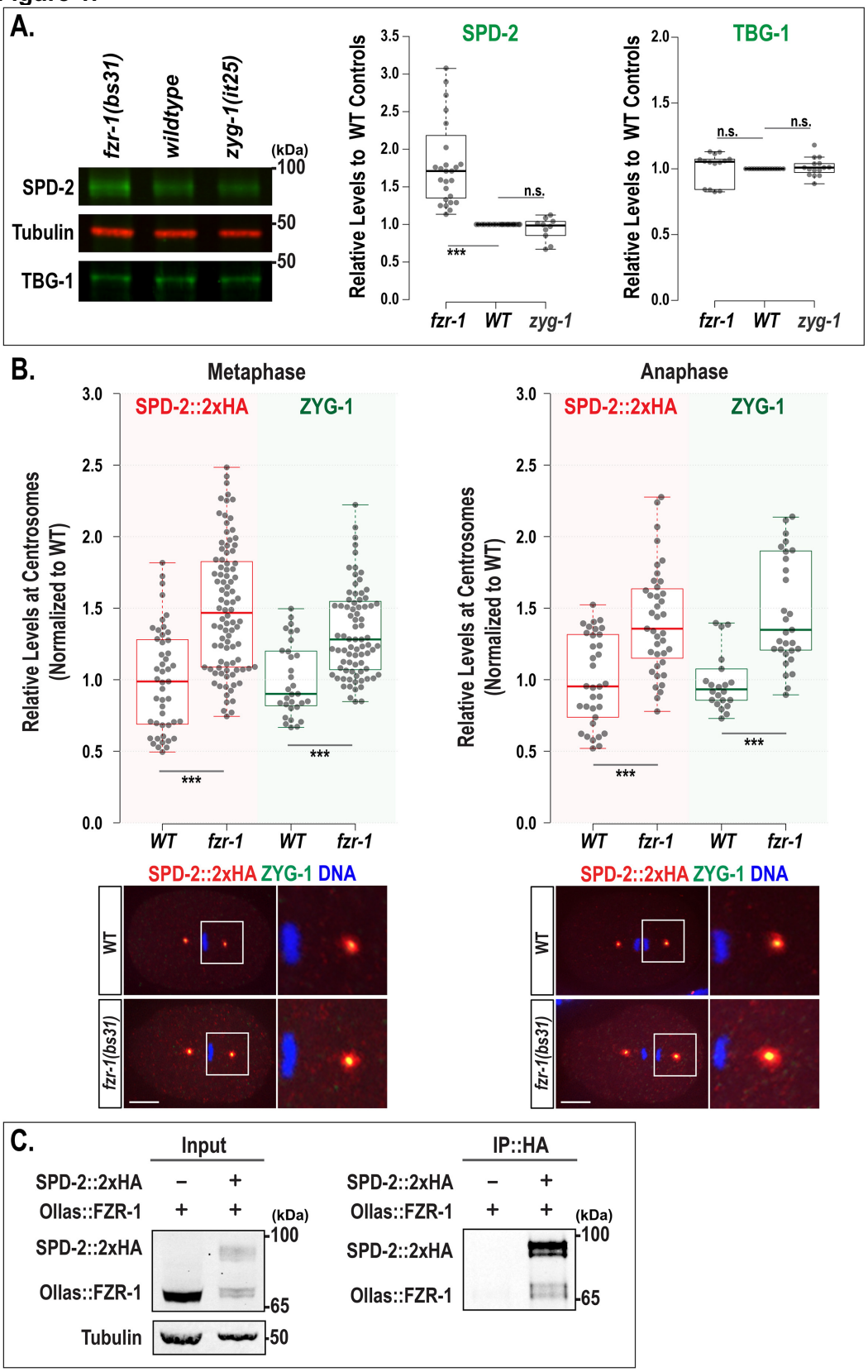

Figures 1-4 Yim et al. 2025

Figure 2.

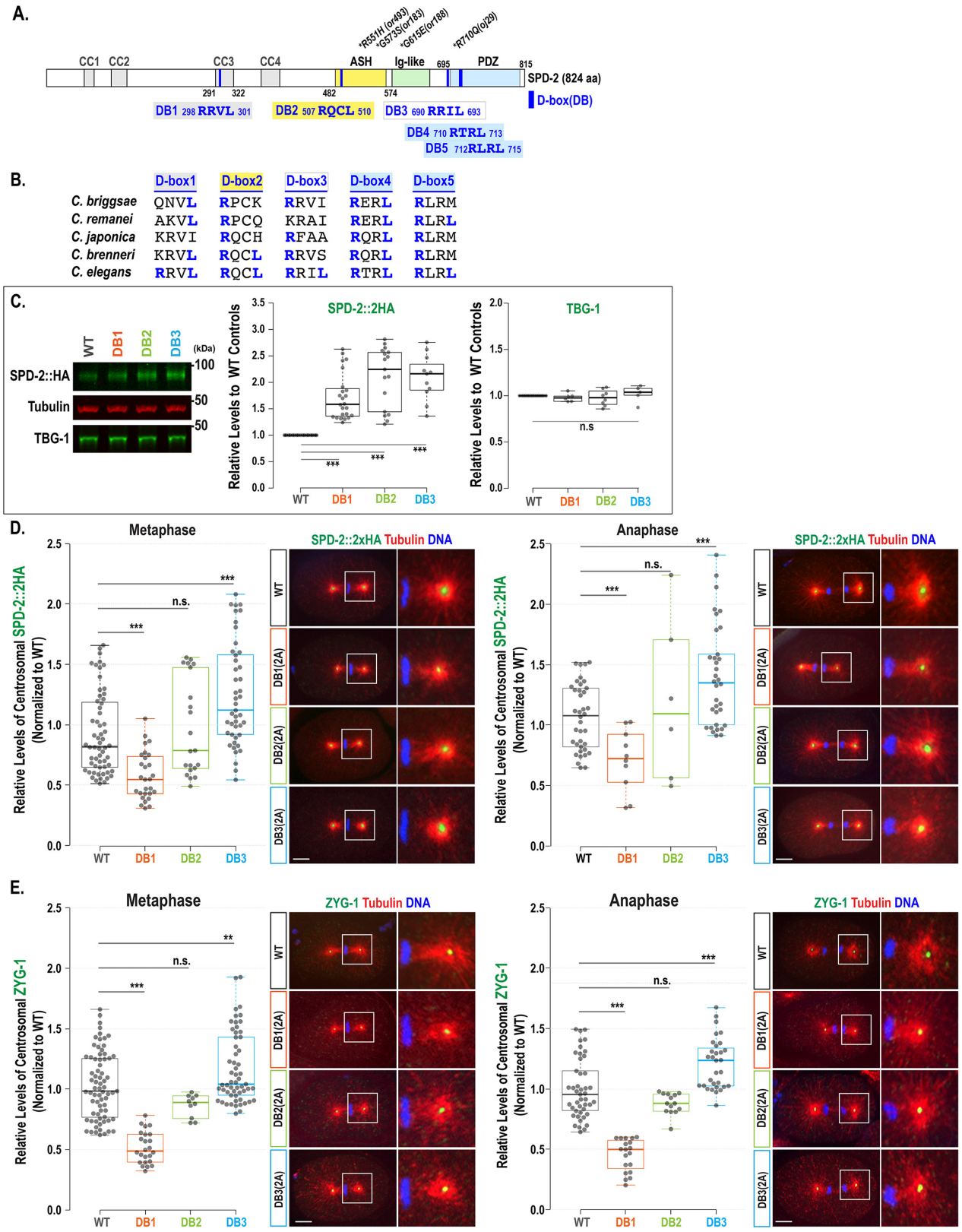

Figures 1-4 Yim et al. 2025

Figure 3.

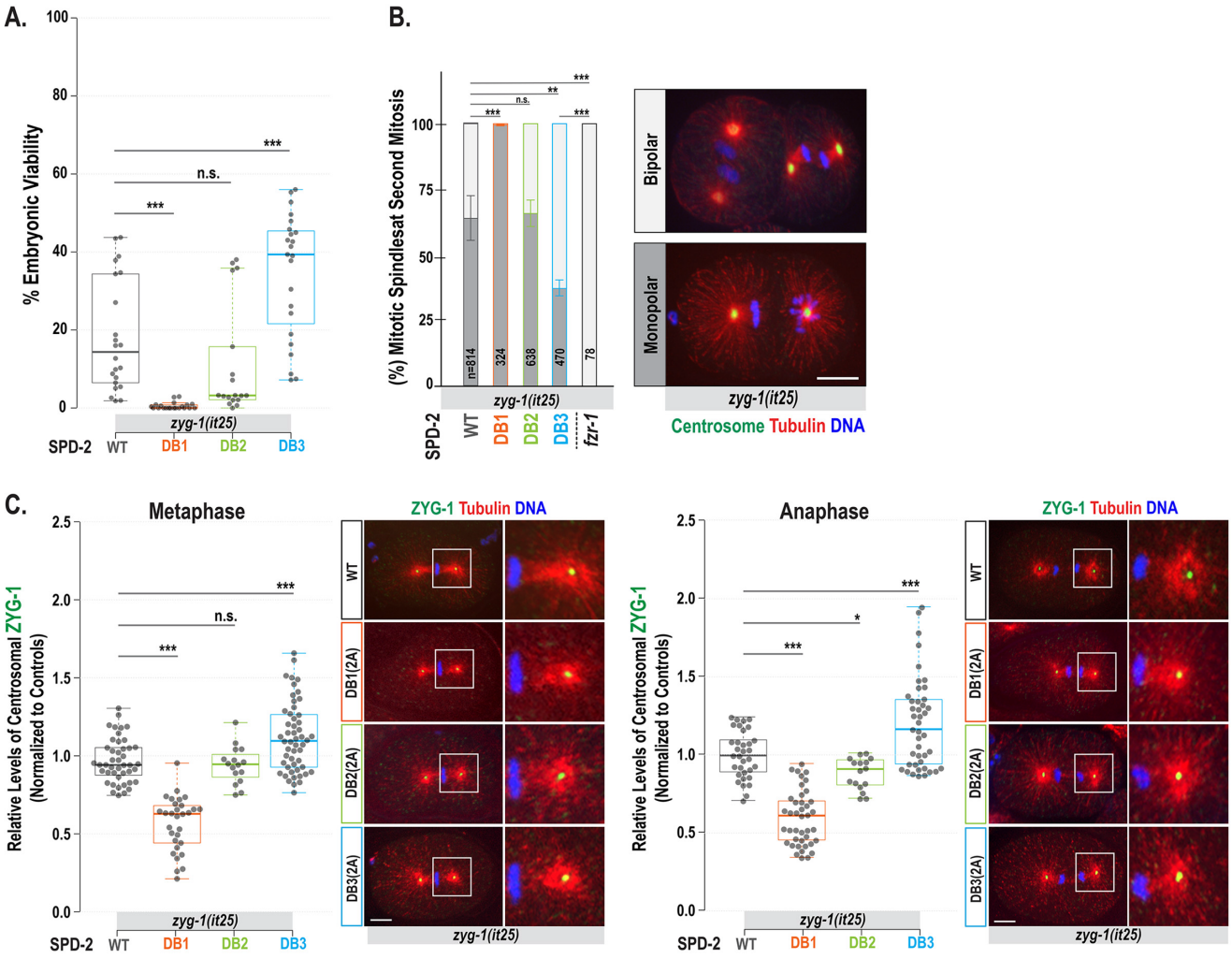

Figures 1-4 Yim et al. 2025
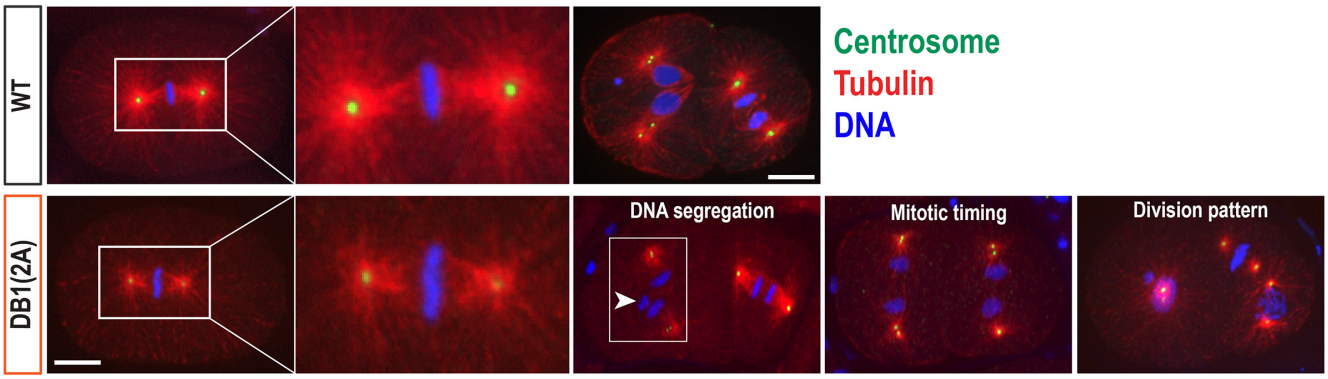
Figure 4.